Flexible, ultrathin and light films from one-dimensional nanostructures of polypyrrole and cellulose nanofibers for high performance electromagnetic interference shielding

Flexible, ultrathin and light films from one-dimensional nanostructures of polypyrrole and cellulose nanofibers for high performance electromagnetic interference shielding

Tomáš Lapka[a], Jarmila Vilčáková[b], Dušan Kopecký[a], Jan Prokeš[c], Marcela Dendisová[a], Robert Moučka[b], Michal Sedlačík[b], Fatima Hassouna[a,*]

[a]*Faculty of Chemical Engineering, University of Chemistry and Technology, Prague, 166 28 Prague 6, Czech Republic*

[b]*Centre of Polymer Systems, Tomas Bata University in Zlín, 760 01 Zlín, Czech Republic*

[c]*Faculty of Mathematics and Physics, Charles University, 180 00 Prague 8, Czech Republic*

[*]*Corresponding author. E-mail address: fatima.hassouna@vscht.cz (F. Hassouna).*

ABSTRACT

Combining highly conducting one-dimensional nanostructures of polypyrrole with cellulose nanofibers (CNF) into flexible films with tailored electrical conductivity and mechanical properties presents a promising route towards the development of eco-friendly electromagnetic interference shielding devices. Herein, conducting films with a thickness of 140 μm were synthesized from polypyrrole nanotubes ($PPy-NT$) and CNF using two approaches, i.e., a new one-pot synthesis consisting of in situ polymerization of pyrrole in the presence of structure guiding agent and CNF, and a two-step synthesis, in which CNF and $PPy-NT$ were physically blended. Films based on one-pot synthesis ($PPy-NT/CNFn$) exhibited higher conductivity than those processed by physical blending, which was further enhanced up to 14.51 S cm^{-1} after redoping using HCl post-treatment. $PPy-NT/\ CNFi_{„}$ containing the lowest $PPy-NT$ loading (40 wt%), thus the lowest conductivity (5.1 S cm^{-1}), displayed the highest shielding effectiveness of — 23.6 dB (>90 % attenuation), thanks to the good balance between its mechanical properties and electrical conductivity.

Keywords: Cellulose nanofibers, polypyrrole nanotubes, composite films electrical conductivity electromagnetic interference shielding

1. Introduction

The development of highly efficient electromagnetic interference (EMI) shielding materials is important to avert damage to the health of living organisms, malfunction of precise electronic devices, and interception of sensitive information. Undesirable EMI are caused by the growing number of highly integrated circuits used in electronic devices, heavy use of transient power sources, or expansion of wireless communication (**Abbasi, Antunes, & Velasco, 2019**).

Electromagnetic interference shielding refers to protection against electromagnetic radiation by absorption or reflection from the material of a shield, which prevents penetration of electromagnetic waves into the protected equipment (**Chung, 2001**). Typical characteristics of an EMI shielding material include high electrical conductivity and large specific surface area (**Chung, 2020**). Standard shielding structures (e.g., boxes, chassis, cable shields, protective packaging, etc.) are made of conductive materials, most frequently non-magnetic or diamagnetic metals (e.g., copper, aluminum, phosphor bronze, brass, steel, etc.). A common approach also includes the coating of plastic housing or enclosures by a thin layer of metal or metal-oxides by certain deposition techniques (e.g., electrolytic deposition, vacuum metallizing, conductive painting, etc.). These materials and methods have proven over time, however, there is a strong need for modern, lightweight, ultra-thin and easily processable materials which will protect new products of a digital era, namely, flexible and wearable electronics, miniature sensors and transducers, precise measuring instruments, etc. (**Lapka et al., 2021; Maity & Chatterjee, 2016; Mäkelä, Pienimaa, Taka, Jussila, & Isotalo, 1997**).

From this point of view, conducting polymers, especially polypyrrole (PPy), have recently attracted increasing interest as they are able to dissipate and attenuate the electromagnetic radiations in the frequency range from 300 kHz to 300 GHz (radio wave and microwave region) due to their high values of electrical conductivity (usually units of S cm^{-1}) and complex permittivity (real part from tens to hundreds) (**Jiang et al., 2019; Kumar et al., 2019**). A current research focuses on the utilization of one-dimensional (1-D) nanostructures of PPy (e.g., nano- and microtubes, rods, wires, etc.). These structures excel over their non-structured counterparts in values of the specific surface area, electrical conductivity, thermal stability and resistance to an oxidative stress (**Stejskal & Trchová, 2018**). Moreover, PPy 1-D nanostructures are also promising as a cheaper and more readily available substitute of carbon-based nanostructures which are well known in the field of EMI shielding (**Abbasi et al., 2019**). However, unlike conventional thermoplastics and thermosets, PPy suffers from its poor processability using methods such as solution casting and melt-processing (**Müller, Rambo, Recouvreux, Porto, & Barra, 2011**). PPy is insoluble in numerous common solvents (**Parit et al., 2020**) and it has tendency to decompose before attaining its melting temperature (**Petit-Conil et al., 2011**). In order to improve the processability of PPy, it has been integrated into various flexible polymer matrices (**Ebrahimi & Gashti, 2018; Gill et al., 2020; Varshney, Ohlan, Jain, Dutta, & Dhawan, 2014**) including polyester (**Yildiz, Usta, & Gungor, 2012**), polyamide (**Granato, Bianco, Bertarelli, & Zerbi, 2009**) and rubber (**Tjahyono, Aw, & Travas-Sejdic, 2012**).

In order to tackle issues related to the dependence on fossil fuels and their negative impact on the environment, replacement of conventional petroleum-based matrices in the fabrication of EMI shielding composites by renewable, biodegradable, and environmentally friendly polymers became an attractive alternative. In this regard, cellulose nanofibers (CNF) as an abundant natural material have gained substantial attention (**Huang, Liu, Zhang, Zhong, & Li, 2015; Huang, Liu, Zhou, et al., 2015; Liu et al., 2022; Marins, Soares, Fraga, Müller, & Barra, 2014; Yang et al., 2017; Yang et al., 2019**). CNF display outstanding mechanical properties (e.g., Young's modulus up to 250 GPa, intrinsic flexibility, etc.) (**Siqueira, Bras, & Dufresne, 2010**), an excellent optical transparency, high aspect ratio, low density, and smooth and reactive surface. Highly flexible materials can be synthesized when CNF are interwoven (**Du, Zhang, Liu, & Deng, 2017**). CNF are advantageous for the design of PPy-based flexible and lightweight composite films as both components can establish interfacial interactions via a hydrogen bonding. Only limited attempts have been undertaken to prepare $PPy/nanocellulose$-based composites for EMI shielding applications (**Hu et al., 2018**). For instance, Tang et al. developed $PPy/bacteria$ cellulose membranes with shielding effectiveness (SE) of —15 dB in 8.2-12.4 GHz. Lately, Huo et al. developed PPy/bacteria cellulose membranes with improved SE exceeding — 28.5 dB in the whole X band (8.2-12.4 GHz) (**Huo et al., 2022**). Gopakumar et al. developed 1 mm thick

PPy/CNF paper with SE of — 22 dB in 8.2-12.4 GHz. More recently, Parit et al. reported on the preparation of PPy/CNF film with a thickness of 138 μm, conductivity of 8.4 S cm^{-1} and SE of — 23 dB in 8-12 GHz. In another study, Chen et al. developed PPy/regenerated cellulose films with conductivity of 0.08 S cm^{-1} and SE of —12.5 dB. Most of PPy/CNF flexible composites are prepared by in situ polymerization of PPy in the non-structured, so-called, globular form (**Gopakumar et al., 2021; Lay, Mendez, Delgado-Aguilar, Bun, & Vilaseca, 2016; Parit et al., 2020**). Recently, 1-D nanostructures of PPy have been found to be promising in nanocellulose composites for the EMI shielding owing to their high aspect ratio, which allows attaining the percolation threshold at a lower loading of PPy filler in a matrix (**Moučka, Sedlačík, Kasparyan, et al., 2020**). **Hu et al.** (**2018**) explored SE of PPy rods in the range of 8-18 GHz. **Xie et al.** (**2017**) examined SE of helical PPy nanostructures, which exhibited SE above —10 dB in the range of 2-18 GHz. SE of $PPy-NT$ has been studied in details (**Babayan, Kazantseva, Moučka, & Stejskal, 2017; Moučka, Sedlačík, Kasparyan, et al., 2020; Moučka, Sedlačík, Prokeš, et al., 2020**) in the C-band range of 5.85-8.2 GHz, where $PPy-NT$ incorporated into sawdust composite exhibited SE of — 20 dB with 18 vol% loading (**Babayan et al., 2017**). SE of almost 80 % of EMI in C-band range has been achieved on the composite of $PPy-NT$ dispersed in pol-ydimethylsiloxane matrix (at 5 wt%) (**Moučka, Sedlačík, Kasparyan, et al., 2020**). However, this type of silicon-based composites displayed limitations associated with the deterioration of their mechanical properties at higher $PPy-NT$ loadings (above 5 wt%), and with their relatively high thickness (2 mm thick plate) (**Moučka, Sedlačík, Kasparyan, et al., 2020**). Lately, Lapka et al. prepared 140 im thick free-standing films of $PPy-NT/CNF$ (50 wt% of $PPy-NT$ loading) by physical blending, which consists of mixing previously synthesized $PPy-NT$ with CNF in aqueous medium. The composite displayed conductivity of 1.16 S cm^{-1} and SE close to 80 % of EMI in the region of 5.85-8.2 GHz (**Lapka et al., 2021**). The SE of above mentioned physically blended composite is high when considering the thickness of the film and $PPy-NT$ loading, and when taking into account the fact that CNF were not coated with a conductive layer. On the other hand, the obtained SE remained inferior when compared to the previous studies on electrically conducting polymer/ cellulose flexible films (**Gopakumar et al., 2018; Gopakumar et al., 2021; Parit et al., 2020**) because of the relatively low loading of $PPy-NT$ and the low thickness of the film. Increase of $PPy-NT$ loading would enhance the SE, but would also compromise the flexibility of the composite films. The in situ polymerization of pyrrole into $PPy-NT$ in the presence of CNF at optimal ratio of $PPy-NT$ to CNF may allow overcoming this issue as the surface of CNF would be covered by a conductive layer of $PPy-NT$, and the formed $PPy-NT$ chains should be intertwined with each other, hence providing a continuous conductive pathway.

Following this hypothesis, in this work we developed a novel, simple one-pot synthesis method for preparation of $PPy-NT/CNF$ self-standing films with a thickness of around 140 μm. This method consists of in situ polymerization of pyrrole in the presence of CNF aqueous suspension, and methyl orange. Methyl orange was employed as a structure guiding agent to mediate the morphology of $PPy-NT$ while CNF acted as a substrate, onto which $PPy-NT$ were deposited. To the best of our knowledge, this is the first work that showed the formation of PPy-NT in the presence of a polymeric matrix, e.g., CNF. For comparison, $PPy-NT/CNF$ composite films were prepared also by physical blending. The relationship among the processing methodology, composition ($PPy-NT$ to CNF ratio), morphology, conductivity, SE, and mechanical properties of the films was established.

2. Materials and methods

2.1. Materials

CNF suspension (3 wt%, cellulose content >85 %; hemicellulose content >5 %; lignin content <1 %) was kindly provided by Weidmann. Iron(III) chloride hexahydrate, Sodium 4-{[4-(dimethylamino)phenyl] diazenyl}benzene-1-sulfonate (methyl orange) and pyrrole were purchased from Merck. Hydrochloric acid (HCl, 35 %) was purchased from $PENTA$. All chemicals were used as received without any further purification. For all experiments, deionized water was used.

2.2. Experimental methods

2.2.1. Materials preparation

2.2.1.1 Synthesis of polypyrrole nanotubes

Synthesis of $PPy-NT$ was carried out following the experimental protocol that we have established previously (**Kopecký et al., 2017; Lapka et al., 2021**). In brief, 600 ml of an aqueous solution containing methyl orange (2.5 mM) and pyrrole (0.05 mM) were first cooled down to 4 °C. 69 ml of iron(III) chloride hexahydrate aqueous solution (0.12 g ml^{-1}) was then added dropwise to the reaction mixture and left under stirring for a day. Product of the reaction was washed several times before drying in a vacuum oven at 40 °C.

2.2.1.2. Preparation of PPy-NT/CNF composite films by physical blending

The $PPy-NT/CNF$ films were prepared by physical blending of $PPy-NT$ and CNF, followed by film formation via solution casting. First, CNF concentration was adjusted to 1 wt%. Then, $PPy-NT$ powder was milled for 2 min at a milling speed of 20,000 rpm (IKA Batch mill Tube Mill 100) and subsequently added into the CNF suspension. After thorough mixing, the resulting suspension was sonicated with an ultrasonic probe (Bandelin HD 4050) during 30 min, at a power of 40 W. Afterwards, the suspension was casted on a Teflon fabric and left to dry at room temperature for several days. After drying a flexible black $PPy-NT/CNF$ thin self-standing film was obtained. The $PPy-NT/CNF$ films with different weight ratios of $PPy-NT$: CNF were elaborated, i.e., 40:60, 50:50, 60:40 and 70:30. The sample designation was defined as $PPy-NT/\ CNF$pb followed by the ratio in w/w % of $PPy-NT$: CNF, e.g. $PPy-NT/\ CNFPB$ 50/50. Abbreviation "PB" in the sample designation refers to the use of physical blending.

2.2.1.3. Preparation of PPy-NT/CNF composite films by in situ polymerization

The elaboration of $PPy-NT/CNF$ films was also carried out by in situ polymerization of pyrrole monomer in the presence of CNF and methyl orange. First, 65.5 mg of methyl orange were dissolved in 50 ml of distilled water. Subsequently, 0.35 ml of pyrrole were added into the reaction mixture. A specific amount of CNF based on the desired ratio pyrrole: CNF was added to the reaction mixture. The suspension was magnetically stirred at 600 rpm. In parallel, 3.4 g of iron(III) chloride were dissolved in 50 ml of distilled water. Both solutions were placed in an ice bath. After reaching a temperature of 4 °C, iron(III) chloride solution was added dropwise into the reaction mixture. The polymerization took place overnight in the ice bath. The resulting suspension was filtrated and washed with water several times. Approximately 70 ml of distilled water were added into the washed and filtered slurry and

sonicated during 30 min (PS 3000, PowerSonic) at room temperature. After that, the suspension was casted on a Teflon fabric and left to dry at room temperature for several days. Smooth black thin films with ratios $PPy - NT$: CNF of 40:60, 50:50, 60:40 and 70:30 were obtained. The sample designation was defined as $PPy - NT/CNF_{in}$ followed by the ratio in w/w % of $PPy - NT$: CNF, e.g., $PPy - NT/CNF_{in}$ 50/50. Term "in" in the sample designation refers to the use of in situ polymerization approach.

2.2.1.4. HCl treatment of PPy-NT/CNF films

HCl treatment of PPy-NT/ CNF films was carried out on films prepared by both physical blending and in situ polymerization. Dry films were immersed into 1 M HCl solution for a period of 1 min. Subsequently, the wet films were pressed using a hydraulic press (H-62, Trystom) with pressure force of 60 kN and left to dry at room temperature. The samples treated with this procedure are marked with "after HCl treatment" in the ending of sample designation.

2.2.2. Characterization

2.2.2.1. Raman spectroscopy

Raman spectroscopy measurements were performed by a dispersive Raman spectrometer with the microscope InVia Reflex (Renishaw, United Kingdom). Excitation wavelength at 785 nm with laser power of 2 mW was applied. Ten accumulations taking 30 s were recorded for one acquisition. The final spectrum was determined as an average of 10 acquisitions.

2.2.2.2. X-ray photoelectron spectroscopy

X-ray photoelectron spectroscopy (XPS) measurements were carried out by Omicron Nanotechnology XPS spectrometer composed of monochromatic radiation Al lamp (1486.7 eV) in the constant analyzer energy mode. The measured spectra were deconvoluted with CasaXPS software.

2.2.2.3. Scanning electron microscopy

The morphological analyses were carried out using a scanning electron microscope (SEM) model Mira 3 LMH (Tescan). All films were analyzed under 3 kV of accelerating voltage.

2.2.2.4. Measurement of electrical conductivity

Electrical conductivity of the films was measured at room temperature by a four-point method in the van der Pauw contact arrangement (**van der Pauw, 1958**) using a Keithley 6221 DC and AC Current Source, a Keithley 2001 Multimeter as a voltmeter and a Keithley 7001 Switch System equipped with a Keithley 7011-S Quad 1 × 10 Multiplexer. Values of conductivities are provided with approx. 5 % accuracy. The detailed measurement procedure is described by **Varga et al.** (**2017**).

2.2.2.5. Tensile testing

A tensile test was carried out on a Testometric universal-testing machine of type M 350-5CT (Testometric Co. Ltd.), equipped with a load cell of 100 N. The tensile properties of the films were investigated using a crosshead speed of 0.5 mm min^{-1} and the length of the gauge equaled 50 mm. Three samples were taken from each group for measurement, and the average value of the calculation is reported. Young's modulus of tensile elasticity (E-modulus) was evaluated as a linear part of the tensile curve in the range of 0.05-0.25 % (according to the standard).

2.2.2.6. Measurement of shielding effectiveness

The SE of the studied composite materials was measured using a PNA-L network analyzer (Agilent N5230A) and rectangular waveguides in the Ku-band (WR 62, i. e., from 12.4 to 18 GHz). Prepared films were cut into rectangular samples with dimensions matching the cross-section of respective waveguides (WR 137 34.85 × 15.80 mm^2 and WR 62 15.8 × 7.9 mm^2). During the waveguide measurement, the samples were positioned with the waveguide's flange and perpendicular to the waveguide's axis (direction of the transmitted wave). The electromagnetic wave is partially transmitted through the sample of given thickness. The employed coaxial transmission line method modified for rectangular waveguides is described in **Mathur and Raman** (**2020**) in details. Shielding effectiveness of the measured sample is expressed in terms of the magnitude of scattering parameter S21 (dB), which returns the portion of transmitted signal at the given frequency calculated according to Eq. **1**.

$$S_{21}\,(\mathrm{dB}) = 20log\frac{I_T}{I_0}, \qquad (1)$$

where I_T and I_0 are intensities of the transmitted and incident electromagnetic wave respectively.

3. Results and discussion

3.1. Morphology

CNF used in this study were obtained by delamination of wood pulp using mechanical pressure processing. The chemical structure, morphology and solid state properties of CNF used in this study as a mechanical support enabling formation of flexible free-standing film were investigated in our previous work (**Lapka et al., 2021**). SEM and TEM images revealed a long fibrillary morphology of CNF with an average diameter of 35 nm. X-ray diffraction (XRD) pattern showed a typical cellulose-I structure, which was in a good accordance with Fourier Transform Infrared ($FTIR$) analysis.

The SEM micrographs of the films at various $PPy-NT$: CNF ratios are depicted in **Fig. 1**. The pure CNF film (**Fig. 1**a) exhibited a compact structure of interconnected nanofibers. $PPy-NTs$ used for the preparation of the films by physical blending (**Fig. 1**b) displayed a nanotubular morphology (several micrometers long with a diameter around 150 nm), indicating that methyl orange played successfully a role of a structure-guiding agent. The structure of the films prepared by physical blending (**Fig. 1**c, d, e and f) showed the co-existence of $PPy-NT$ and CNF, and morphological discrepancies associated with the material composition (ratio between PPy-NT and CNF). The film $PPy-NT/CNFPB$ 40/60 (**Fig. 1**c) is characterized by a compact structure, in which CNF and $PPy-NT$ are highly entangled and interconnected among themselves due to the establishment of large intermolecular hydrogen

bonding interactions (**Johnston, Moraes, & Borrmann, 2005**). Indeed, $PPy-NT$ interact with CNF via the hydrogen bonding, which take place between amine groups of the pyrrole ring and hydroxyl groups of the cellulose moiety.

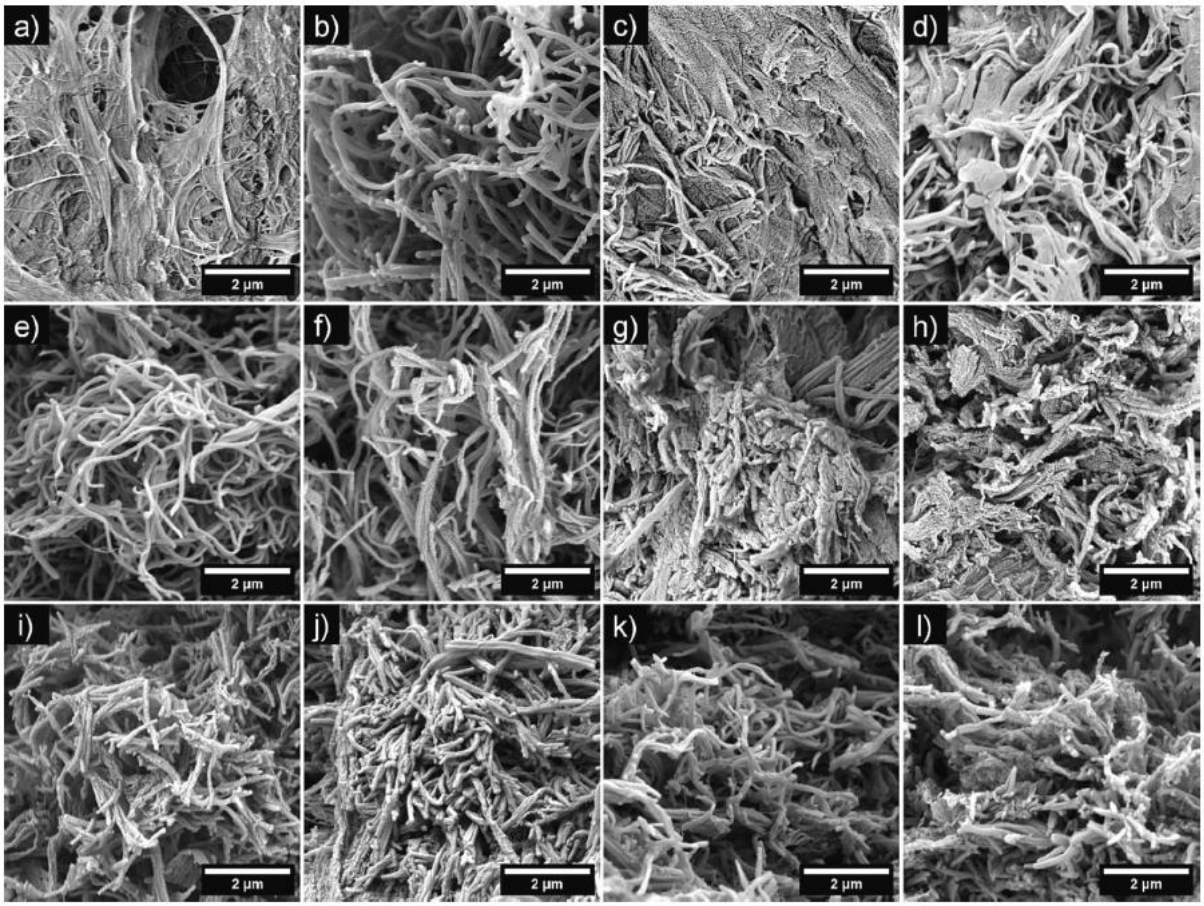

Fig. 1. SEM images of a) CNF film, b) $PPy-NT$, c) $PPy-NT/CNF_{pB}$ 40/60, d) $PPy-NT/CNF_{pB}$ 50/50, e) $PPy-NT/CNF_{pB}$ 60/40, f) $PPy-NT/CNF_{pB}$ 70/30, g) $PPy-NT/\ CNF_{in}$, 40/60, h) $PPy-NT/CNF_{in}$ 50/50, i) $PPy-NT/CNF_{in}$ 60/40, j) $PPy-NT/CNF_{in}$ 70/30, k) $PPy-NT/CNF_{PB}$ 50/50 after HCl treatment, and l) $PPy-NT/CNF_{in}$ 50/50 after HCl treatment.

At higher $PPy-NT$ loadings (**Fig. 1**d, e and f), $PPy-NT$ stand out better, and the entangled $PPy-NT/CNF$ network becomes less compact with an open porous structure. The SEM images of the films prepared by in situ polymerization showed the formation of $PPy-NT$ on the surface of CNF. This indicates that methyl orange acted as a conventional primary template, i.e., the structure guiding agent responsible for the nanotubular shape, while CNF played a role of a substrate and secondary template for $PPy-NT$. The $PPy-NT$ become more prominent and better defined with the increase of pyrrole concentration during the polymerization (**Fig. 1**g, h, i, j). A close inspection reveals that the deposition of $PPy-NT$ on the surface of CNF reduced the inter-nanofiber hydrogen bonding interactions, hence resulting in a more intimately entangled and uniform network compared to the films prepared by physical blending. After the HCl treatment, the morphology of all films remained unchanged as can be seen in SEM pictures of selected $PPy-NT/\ CNF$ 50/50 films (**Fig. 1**k and l).

3.2. Chemical structure

The chemical structure of the prepared $PPy-NT/CNF$ films was investigated by means of Raman spectroscopy and XPS. All Raman spectra displayed the same spectral features corresponding to $PPy-NT$ in the used excitation mode of 785 nm (in resonance with the energy of delocalized bipolarons and polarons (**Stejskal & Trchová, 2018**)), regardless of the film composition and preparation methodology. For the sake of simplicity, only single composition of $PPy-NT$: CNF equal to 50: 50 w/w % is depicted in **Fig. 2**a. Typical peaks of $PPy-NT$ at 1591 cm^{-1} ($C=C$ stretching), 1383 cm^{-1} (antisymmetrical inter-ring stretching C—N vibration of oxidized, protonated $PPy-NT$), 1325 cm^{-1} (inter-ring stretching $C—C$ vibration mode in neutral states of $PPy-NT$), 1240 cm^{-1} (bending $C—H$), 1080 cm^{-1} ($C—H$ in-plane deformation with oxidized; protonated species), 1050 cm^{-1} ($C—H$ in-plane deformation; non-protonated $PPy-NT$ units), 976 and 933 cm^{-1} (ring in-plane deformation belonging to polaron and bipolaron states of $PPy-NT$, respectively) (**Minisy et al., 2020; Stejskal & Trchová, 2018)**. In the Raman spectra of the films, no shift corresponding to CNF or methyl orange was detected at a laser excitation line of 785 nm since this excitation line falls in the polaron absorption band of PPy and the depth of penetration is only about several nanometers (close to the surface) (**Minisy et al., 2020**). Raman spectroscopy results suggest that $PPy-NT$ generated in situ in the presence of CNF and methyl orange dye, namely, in situ polymerization, has the same chemical structure as the $PPy-NT$ powder used to prepare $PPy-NT/CNF$ films by physical blending. It is worth mentioning that the Raman shifts of CNF (see **Fig. 2**b) are not observed in the Raman spectra of $PPy-NT/CNF$ films due to the used 785 nm laser excitation line, which is in resonance with the energy of delocalized bipolarons and polarons of $PPy-NT$ (**Stejskal & Trchová, 2018**).

The XPS wide-survey spectra confirmed the surface deposition of $PPy-NT$ on CNF in the composites prepared by the in situ polymerization. The atomic proportion of the elements presented at the surface of the prepared films and the reference $PPy-NT$ powder are summarized in **Table 1** and Fig. S1. The XPS analysis of $PPy-NT$ powder used to prepare the films by physical blending reveals the presence of five main peaks at binding energies of about 285, 400, 532, 198 and 168 and 198 eV, attributed to carbon (C(1s)), nitrogen (N(1s)), oxygen (O(1s)), chlorine (Cl) and sulfur (S(1s)) atoms, respectively.

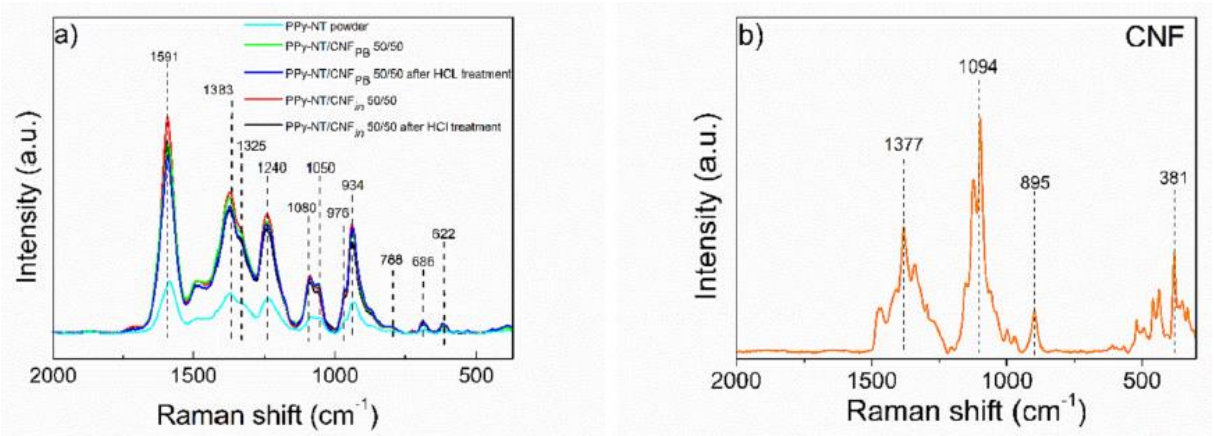

Fig. 2. Raman spectra of a) $PPy-NT$ powder and representative $PPy-NT/CNF$ films, and b) CNF.

Table 1 Summary of XPS data of $PPy-NT$ powder and $PPy-NT/CNF$ films: atomic proportions.

	C (%)	O (%)	N (%)	S (%)	Cl (%)
Binding energy (eV)	285	532	400	168	198
PPy-NT powder	74.1	9.6	12.0	1.6	2.7
PPy-NT/CNF_{PB} 50/50	59.7	35.9	3.2	0.7	0.5
PPy-NT/CNF_{in} 40/60	63.3	28.7	5.7	–	2.3
PPy-NT/CNF_{in} 50/50	66.0	22.3	8.4	–	3.3
PPy-NT/CNF_{in} 60/40	69.7	19.2	8.3	–	2.9
PPy-NT/CNF_{in} 70/30	68.7	18.4	9.6	–	3.3

The N(1s) and C(1s) belong to PPy-NT and methyl orange. The S(1s) and O(1s) belong to methyl orange remaining on the surface while the presence Cl is caused by residues of iron(III) chloride. Survey spectra of the films prepared by in situ polymerization (**Table 1** and Fig. S2) indicate the decrease of O(1s) and the increase of the N(1s) proportions with the increase of PPy-NT loading. The higher proportion of O(1s) observed at lower $PPy-NT$ loading (i.e., below 60 wt% of $PPy-NT$) comes from CNF surface hydroxyl groups. For equivalent composition, e.g., $PPy-NT$:CNF equal to 50:50 % w/w (**Table 1**) and comparatively to the composite obtained by the in situ polymerization, the one prepared by physical blending exhibits higher proportion of O(1s), partly coming from the CNF surface, since in this case CNF is solely physically entangled with $PPy-NT$.

In order to establish the redox and protonation state of $PPy-NT$, high resolution spectra of N1(s) were deconvoluted (Fig. S2 and **Table 2**). The deconvolution of N(1s) core level spectra for $PPy-NT$ powder and the films shows the presence of three main peaks at binding energies of 399.47, 400.73 and 402.05 eV attributed to pyrrolic nitrogen ($-N-H-$), protonated cation nitrogen ($-N-H^{+}$-; polaron), and protonated nitrogen ($=N-H^{+}$-; bipolaron), respectively (**Ciric-Marjanović et al., 2014**; **Han & Cho, 2018; Lapka et al., 2021; Minisy et al., 2019**).

Table 2 Summary of XPS data of $PPy-NT$ powder and $PPy-NT/CNF_{in}$: proportion of nitrogen.

	–N—H– (%)	–N—H^{+}– (%)	=N—H^{+}– (%)
Binding energy (eV)	399.57	400.73	402.05
PPy-NT powder	66.9	26.6	9.5
PPy-NT/CNF_{in} 40/60	64.4	25.1	10.5
PPy-NT/CNF_{in} 50/50	70.2	18.8	11.0
PPy-NT/CNF_{in} 60/40	68.9	23.1	8.0
PPy-NT/CNF_{in} 70/30	66.8	19.5	13.8

The $PPy-NT$ present in films prepared by in situ polymerization exhibits comparable proportions of nitrogen moieties and a protonation level of about 35 $\pm$ 5 % with that of PPy-NT powder used to prepare the films by physical blending.

3.3. Electrical conductivity

High electrical conductivity is a prerequisite for the design of EMI shielding materials. Conductivity of $PPy-NT/CNF$ films at various $PPy-NT$: CNF ratios was measured and the values are summarized

in **Fig. 3**. Conductivity of both types of films (i.e., $PPy-NT/CNF_{PB}$ and $PPy-NT/\ CNF_{in}$) increases with the increase of $PPy-NT$ loading. The conductivity of the films is enhanced by the HCl treatment, hence indicating an effective redoping of $PPy-NT$ by the strong inorganic acid (**Ayad, 1994; Goel, Mazumdar, & Gupta, 2010; Hawkins & Ratcliffe, 2000**). This redoping effect using HCl solution at concentration below 3.5 M to avoid degradation of PPy was previously reported in the literature (**Ayad, 1994; Goel et al., 2010**). Nevertheless, conductivity remains lower than that of $PPy-NT$ powder (60 S cm^{-1}) due to the electrically insulating properties of CNF. For equivalent composition, the films prepared by in situ polymerization exhibit superior conductivity than those obtained by physical blending. For instance, conductivity of $PPy-NT/CNF_{PB}$ 70/30 and $PPy-NT/CNF_{in}$ 70/30 is 3.71 and 6.52 S cm^{-1}, respectively, and it upshifted to 8.99 and 14.51 S cm^{-1}, respectively, after the HCl treatment.

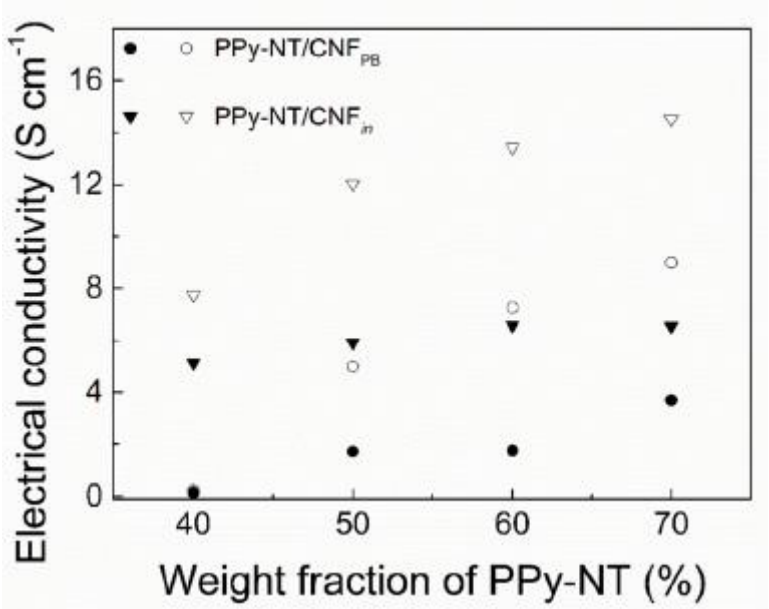

Fig. 3. Conductivity of $PPy-NT/CNF$ films before (closed symbols), and after (open symbols) the HCl treatment.

This is likely due to the fact that in situ polymerization results in a thorough and homogenous coating of $PPy-NT$ on the surface of CNF as attested by SEM and XPS analysis, leading to the formation of $PPy-NT$ chains intertwined with each other, and hence providing a continuous and compact conductive pathway (**Lay, Méndez, Delgado-Aguilar, et al., 2016**).

Compared to most of the studies reported in the literature (**Huo et al., 2022; Lay, Méndez, Pelach, Bun, & Vilaseca, 2016; Jradi, Bideau, Cha-bot, & Daneault, 2012**), our one-pot synthesis method, i.e., so-called in situ polymerization approach, led to superior conductivity for CNF and conducting polymers-based composite films. Using this new method, supramolecular structures of $PPy-NT$ are generated and uniformly deposited on the surface of CNF in the presence of a structure guiding agent, thereby resulting in the formation of a continuous conductive network pathway (**Gopakumar et al., 2021; Parit et al., 2020**).

3.4. Mechanical properties

Besides conductivity, the SE of $PPy-NT$ in the $PPy-NT/CNF$ composite film depends on the mechanical properties of the latter. The $PPy-NT$ was incorporated into CNF to enhance its mechanical properties and processability. The CNF acts as a flexible skeleton with high tensile modulus capable of high deformation (**Moohan et al., 2020**). The outstanding mechanical performance of CNF is attributed to the geometry of fibrils, which are composed of individual cellulose molecules in extended-chain conformation, and also to stiffness of cellulose (**Wang, Miao, Li, & Chen, 2022**). Its high tensile modulus is commonly assigned to the ordered structure of cellulose, and especially to its intricate hydrogen bonding network (**Altaner, Thomas, Fernandes, & Jarvis, 2014; Moon, Martini, Nairn, Simonsen, & Youngblood, 2011**). The impact of the composition (i.e., ratio between $PPy-NT$ and CNF) and the strategy used to prepare the composites (i.e., in situ polymerization or physical blending) on the mechanical properties of 140 |im thick $PPy-NT/CNF$ films was assessed.

Based on the stress-strain curves (Fig. S3a), all mechanical properties of $PPy-NT/CNF_{in}$ films like the elastic modulus (**Fig. 4**a), ultimate tensile strength (**Fig. 4**b) and elongation at break (**Fig. 4**c) improved with the increase of the CNF loading.

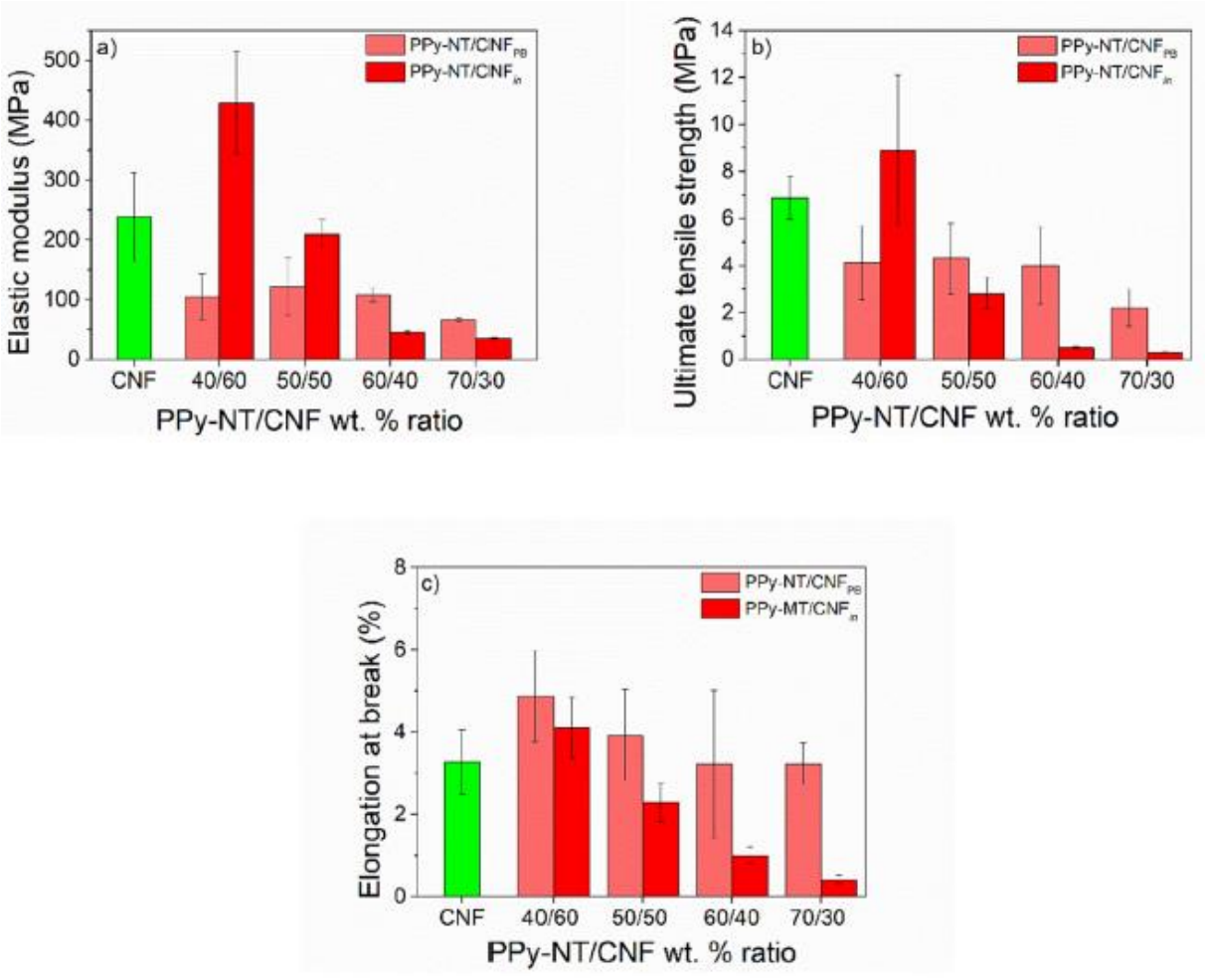

Fig. 4. Mechanical properties of $PPy-NT/CNF$ films: a) elastic modulus, b) ultimate tensile strength, and c) elongation at break.

For instance, the $PPy-NT/CNF_{in}$ 40/60 composite with the highest CNF loading exhibited the uppermost tensile strength (9 $\pm$ 3 MPa), elastic modulus (429 $\pm$ 85 MPa), and elongation at break (4

$\pm$ 1 %), resulting in better flexibility and mechanical strength of the film, comparable to those of pure CNF film (Figs. S3 and S4). These properties dropped significantly down at higher $PPy-NT$ loading, resulting in brittle films. Generally, a higher content of CNF in the composite enhances the elastic modulus and tensile strength due to the enhanced hydrogen bonding among CNF. Meanwhile, the enhancement of mechanical properties also corresponds to strong interactions between $PPy-NT$ and CNF. While at 40 wt% of $PPy-NT$, a balance of inner CNF interactions and interaction between CNF and $PPy-NT$ chains was probably achieved, but not in the case of a higher $PPy-NT$ loading. Indeed, a large surface coating of $PPy-NT$ on CNF has tendency to reduce the intermolecular hydrogen bonding interactions among CNF, which restricts significantly their movement, thereby hindering their flexibility.

While a clear trend between the composition and mechanical properties was observed for $PPy-NT/CNF_{in}$, this is not completely the case for $PPy-NT/CNF_{pB}$ (Fig. S3b, **Fig. 4**a, b and c). Indeed, the increase of $PPy-NT$ loading from 40 to 60 wt% did not affect mechanical properties of the $PPy-NT/CNF_{PB}$ films noticeably (within the standard deviation) as they all exhibited comparable elastic modulus (112 $\pm$ 32 MPa), tensile strength (4 $\pm$ 2 MPa) and elongation at break (4 ± 1 %). At the highest PPy-NT loading (i.e., 70 wt%), elastic modulus and tensile strength dropped down to 66 ± 3 MPa and 2 $\pm$ 1 MPa, respectively, making this formulation more brittle. Overall, for equivalent composition, mechanical properties of $PPy-NT/CNF_{PB}$ are superior to $PPy-NT/CNF_{in}$ except for $PPy-NT/CNF_{in}$ 40/60, which exhibited by far the best mechanical performance. Unlike in $PPy-NT/CNF_{in}$, CNF is only physically entangled with $PPy-NT$ in $PPy-NT/CNF_{PB}$. It means that although there is a significant restriction of CNF motion with the increase of $PPy-NT$ loading, intermolecular hydrogen bonding interactions between CNF did not completely vanish, thereby allowing the flexibility of the films to be maintained (particularly up to 60 wt% of $PPy-NT$). However, the hydrogen bonding interactions between $PPy-NT$ and CNF are not as strong as in case of $PPy-NT/CNF_{\text{in}}$, which is not in a favor of the improved mechanical performance. This may explain the superior mechanical properties of $PPy-NT/CNF_{in}$ 40/60 over all PPy-NT/CNFPB films, as it exhibited a balance of strong interactions between CNF (i.e., retention of intermolecular hydrogen bonding), and CNF with $PPy-NT$ (**Parit et al., 2020**).

Except for $PPy-NT/CNF_{in}$ 40/60, the HCl treatment of all $PPy-NT/\ CNF_{in}$ and $PPy-NT/CNF_{PB}$ films (Fig. S4 and **Fig. 5**a, b and c) did not change noticeably their mechanical properties since they exhibited similar values of elastic modulus and ultimate tensile strength than before the treatment, within the experimental error. The slight deviation of the elongation at break between the films before and after the HCl treatment is negligible given the very low elongation of the CNF based films. Interestingly, though PPy-NT/CNFn 40/60 treated by HCl still exhibits the best mechanical performance among all compositions prepared using in situ polymerization, elastic modulus and ultimate tensile strength of the former dropped down after the HCl treatment. Owing to the morphological and structural complexity of this formulation, the mechanism responsible for its mechanical deterioration is unclear. However, rearrangement of the chains during the HCl treatment leading to the appearance of micro/nano voids could be at the origin of this performance deficiency (**Ayad, 1994; Cho, Choo, Kim, & Kim, 2007**).

3.5. EMI shielding

As reported in our previous works, one-dimensional PPy structures are very promising for the development of EMI shielding materials thanks to their high aspect ratio and elevated electrical conductivity (**Lapka et al., 2021; Moučka, Sedlačík, Kasparyan, et al., 2020; Moučka, Sedlačík, Prokeš,**

et al., 2020). EMI shielding properties of the $PPy - NT/\ CNF$ films were performed in K_u band, which corresponds to a frequency range of 12.4-18 GHz, and belongs to super high frequency range of radio spectrum.

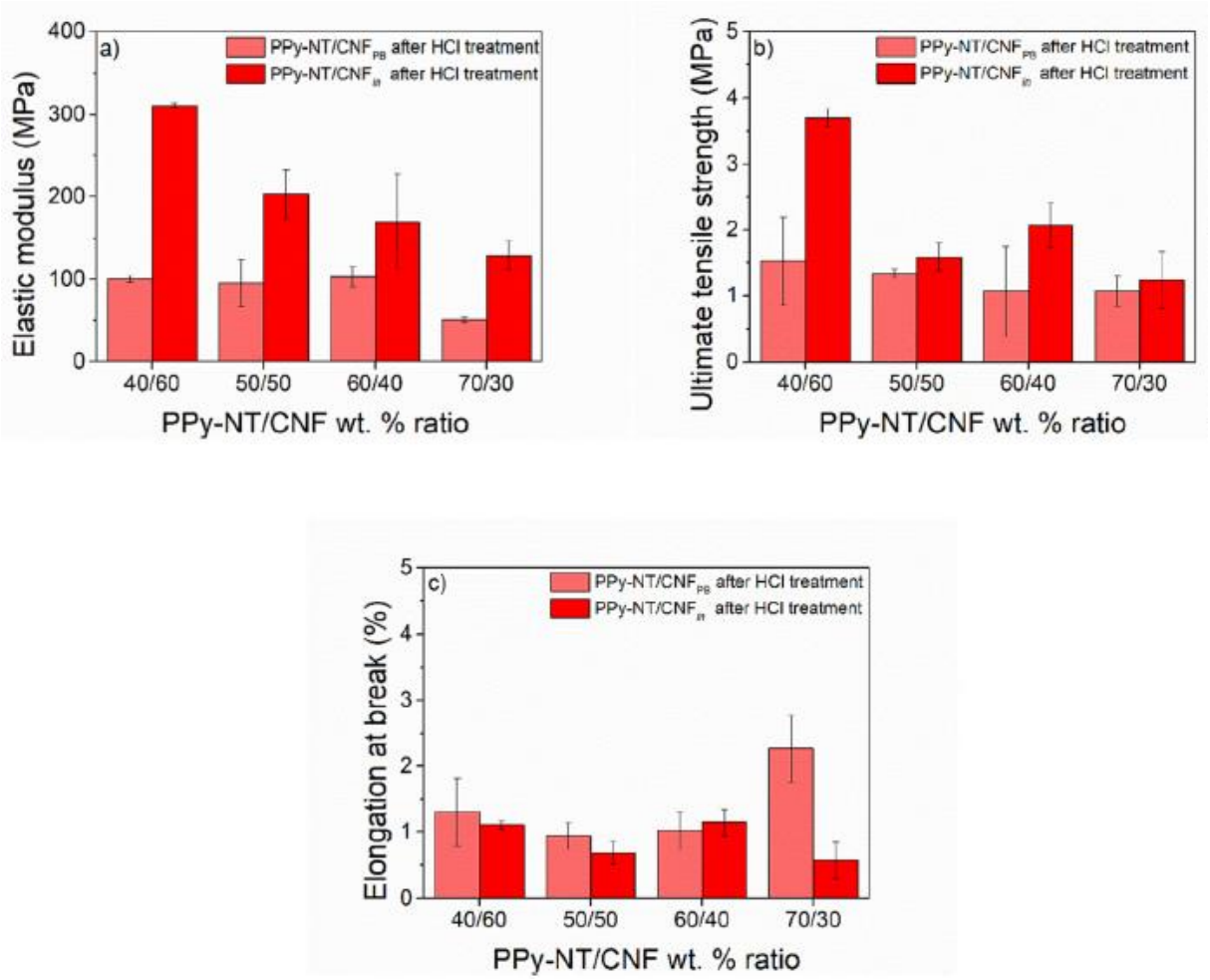

Fig. 5. Mechanical properties of $PPy - NT/CNF$ films after the HCl treatment: a) elastic modulus, b) ultimate tensile strength, and c) elongation at break.

The K_u band is mostly used for satellite communications. EMI is defined as radiated or conducted electromagnetic signal that interferes with the functioning of external electronic devices (**Thomassin et al., 2013**). When an electromagnetic wave meets a surface of a material, it can either be transmitted, reflected or absorbed. Its shielding can be achieved either by absorption or by reflection of the electromagnetic signal (**Chung, 2020**).

As can be expected, the SE value of CNF film is close to zero (**Fig. 6**a, c and **Fig. 7**a, c) due to its electrically insulating nature, which transmits most of the electromagnetic energy. The SE of $PPy - NT/CNF_{PB}$ illustrated in **Fig. 6**a and b increases with the increase of $PPy - NT$ loading up to 60 wt%, reaching a maximum of —11.8 dB in K_u band (74.3 % attenuation) with $PPy - NT/CNF_{PB}$ 60/40. Despite its highest electrical conductivity among all $PPy - NT/CNF_{PB}$ films, $PPy - NT/CNF_{PB}$ 70/30 exhibits low SE comparable to the film containing the lowest $PPy - NT$ content (i.e., $PPy - NT/CNF_{PB}$ 40/60). The poor EMI shielding performance of $PPy - NT/\ CNF_{PB}$ 70/30 can be corrected with its poor mechanical properties characterized by high brittleness, so that residual stresses can form micro/nano-cracks. Such cracks worsen SE of the films as they transmit some of the electromagnetic radiation encountered by the material (**Chung, 2020**). On the other hand, further treatment of $PPy -$

NT/CNF_{PB} with HCl leads to the enhancement of SE of the films. In this case, SE follows conductivity of the films, which increases as a function of $PPy-NT$ loading. Despite its poor mechanical properties, $PPy-NT/CNF_{PB}$ 70/30 after the HCl treatment displays the highest SE with an average SE of —16.6 dB in the K_u band (85.2 % attenuation). The high conductivity exhibited by this film as a result of the HCl treatment must have counterbalanced its poor mechanical properties, hence allowing for enhancement of SE.

Interestingly, no correlation was found between SE (**Fig. 7**) and conductivity (**Fig. 3**) of the $PPy-NT/CNF_{in}$ films. Though $PPy-NT/CNF_{in}$ 40/60 exhibited the lowest conductivity ($\sigma = 5.1$ S cm^{-1}), it displayed the highest SE value of — 23.6 dB, (93.4 % attenuation). SE of this film is higher than the reported literature values of composite films based on PPy/CNF given the low thickness (140 μm) (**Table 3**) and the amount of PPy-NT incorporated inside the film higher than the reported literature values of composite films based on PPy/CNF given the low thickness (140 µm) (Table 3) and the amount of PPy-NT incorporated inside the film.

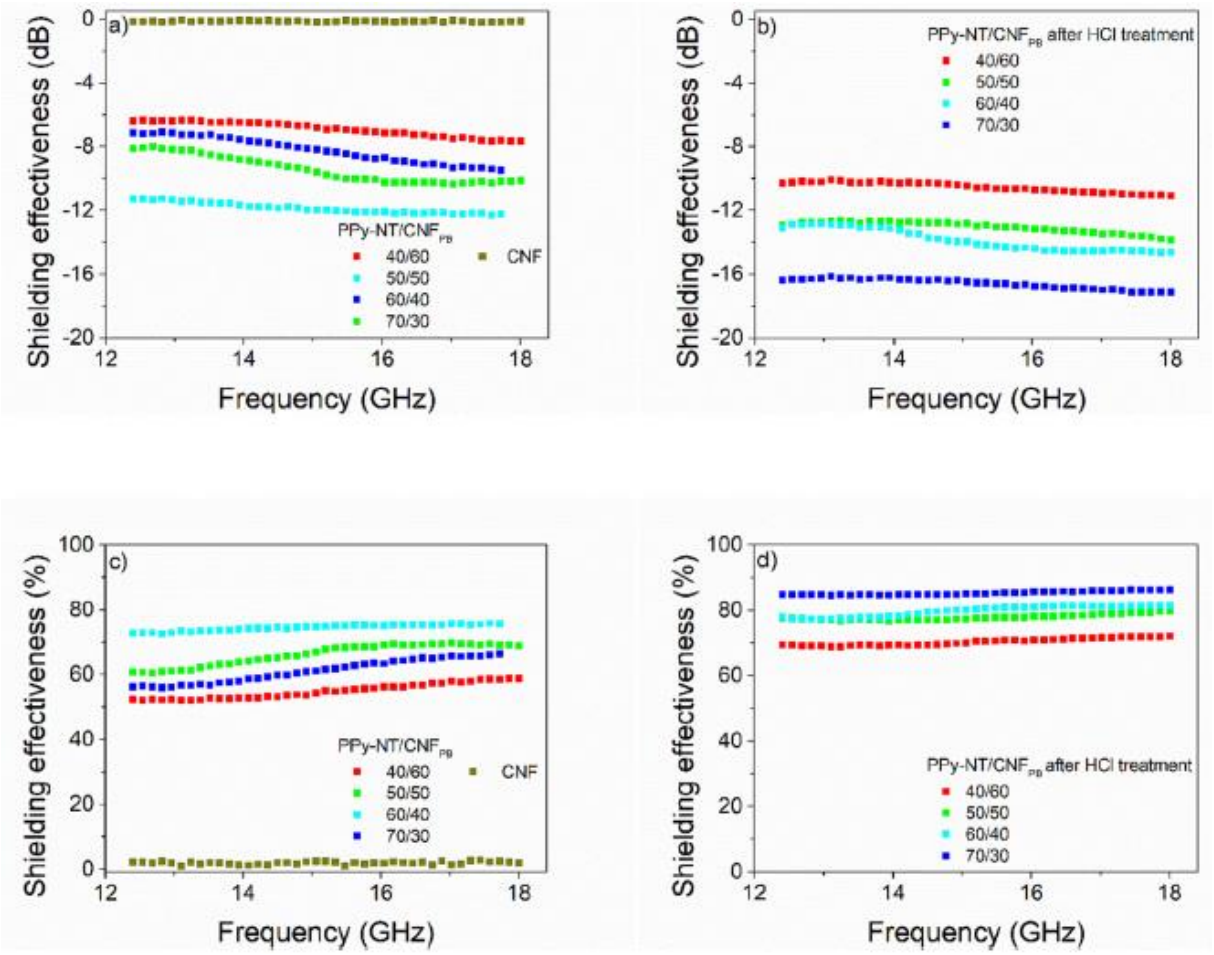

Fig. 6. Results of $EMI\ SE$ of $PPy-NT/CNF_{PB}$ before and after HCl treatment in the K_u band. a) and b) in decibels (dB), and c) and d) converted to percentages.

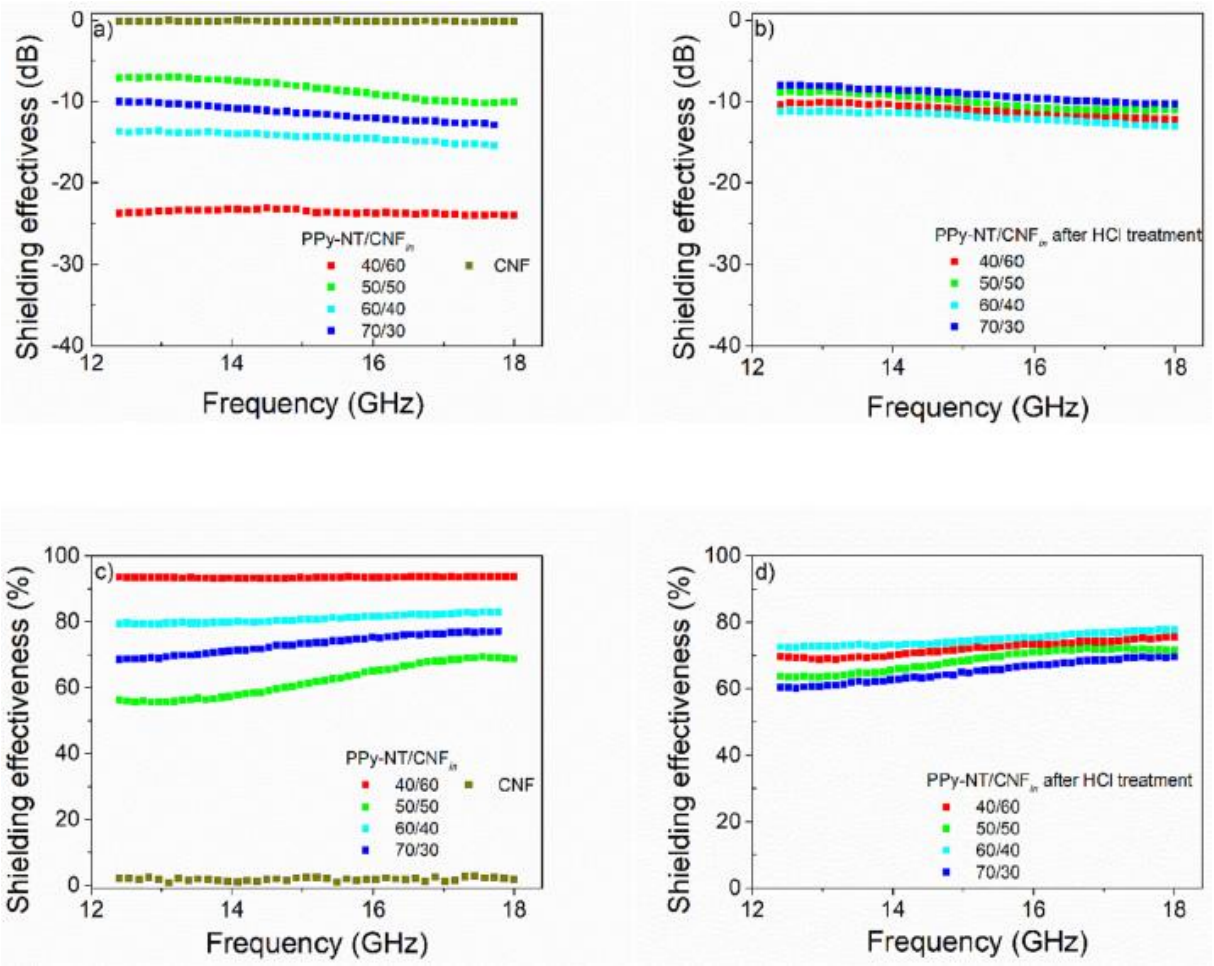

Fig. 7. Results of $EMI\ SE$ of $PPy-NT/CNF_{in}$ before and after HCl treatment in the K_u band. a) and b) in decibels (dB), and c) and d) converted to percentages.

Table 3 Comparison of SE of previously reported entirely organic composites based on PPy/cellulose.

Composite	Thickness (μm)	Frequency (GHz)	SE (dB)	Reference
PPy/bacterial cellulose membrane		0.5–3.0	−15	(Tang, Han, Jiang, Chen, & Wang, 2015)
PPy/CNF thin film	1000	8.2–12.4	−22	(Gopakumar et al., 2021)
PPy/PVA/CNF thin film	138	8.2–12.4	−23	(Parit et al., 2020)
PPy-NT/CNF thin film	140	12–18	−23.6	This study

Moreover, our composite film is advantageous from environmental point of view as it contains preponderant amount of CNF, i.e., 60 wt%. Films with higher $PPy-NT$ loadings, and thus higher conductivity exhibited lower SE in the range from — 7 to —13.8 dB (60 %-80 %). Moreover, post-treatment of films using HCl did not enhanced SE despite superior conductivity values. It even deteriorated SE of $PPy-NT/CNF_{in}$ 40/60 down to 71.3 %. This peculiar behavior of the $PPy-NT/CNF_{in}$ in terms of SE recalls the one of $PPy-NT/CNF_{PB}$ 70/ 30, and it is likely related to the

mechanical properties of the films. Indeed, the film exhibiting the best mechanical properties, i.e., $PPy-NT/\ CNF_{in}$ 40/60, is also the one displaying the highest SE. As aforementioned, at higher $PPy-NT$ loading, the films become brittle, and therefore more prompt to the appearance of micro/nano-cracks under weak/re-sidual stress, thereby leading to a partial transmission of the electromagnetic radiation encountered by the material. Unlike the films prepared by physical blending where the intrinsic properties of CNF playing a role of a flexible matrix are preserved, in the films obtained by in situ polymerization CNF are covered by $PPy-NT$, thus compromising their flexibility at a given $PPy-NT$: CNF ratio, and thus their SE. While the HCl treatment contributed to enhancement of conductivity of all films and SE of the $PPy-NT/CNF_{PB}$ films, it did not help improving SE of $PPy-NT/CNF$;„ because of the worsening of their mechanical performance. Therefore, in order to achieve a composite with high SE, the film must exhibit high conductivity combined with mechanical flexibility.

4. Conclusions

In this study, we developed and compared two types of electrically conducting composite thin films with a thickness of 140 μm from $PPy-NT$ and CNF. Morphological analysis of the newly developed $PPy-NT/\ CNF$;„ composite using a one-pot synthesis via in situ polymerization of pyrrole in the presence of methyl orange and CNF showed the formation of $PPy-NT$ growing on the surface of CNF. Methyl orange acted as a powerful primary template, i.e., the structure guiding agent responsible for the nanotubular shape, while CNF played a role of a substrate and secondary template for PPy. As a result, the films prepared using this new approach exhibited higher conductivity than those processed by physical blending of CNF and pre-synthesized $PPy-NT$, which was further enhanced up to 14.51 S cm^{-1} after redoping using the HCl posttreatment. Using this new method, $PPy-NT$ known to exhibit the best electrical conductivity compared to other PPy shapes, are uniformly deposited on the surface of CNF in the presence of a structure guiding agent, thus ensuing the formation of a continuous conductive network pathway. Thanks to this morphology, the $PPy-NT/CNF_{in}$ 40/60 film, containing the lowest $PPy-NT$ loading of 40 wt%, and thus the lowest conductivity (5.1 S cm^{-1}) displayed the highest SE of — 23.6 dB (>90 % attenuation), due to the good balance of mechanical and electrical conductivity properties exhibited by this film. For equivalent composition, the film prepared by physical blending, i.e., $PPy-NT/CNF_{PB}$ 40/60 displayed lower conductivity and shielding performance as in this case CNF free of conductive layer is only physically and randomly entangled with PPy-NT. Correlation between the electrical conductivity, mechanical properties and EMI shielding performance (frequency range of 12.4-18 GHz) of the films was established. At higher PPy-NT loadings, the films became brittle and therefore more prone to the formation of cracks at weak residual stresses, which can affect negatively SE. However, globally SE of $PPy-NT/CNF_{PB}$ increased with the increase of the electrical conductivity of the films since the mechanical properties of the films were not significantly affected by the increase of $PPy-NT$ loading. For equivalent composition, the mechanical properties of PPy-NT/ CNFpb were superior to $PPy-NT/CNF$;„ except for $PPy-NT/CNF$;„ 40/60, which exhibited by far the best mechanical performance and also the highest SE. The two approaches proposed in this study are both cost-effective and scalable. The properties of the films can be tailored and adjusted to the final application. These cost effective biobased conducting films can find applications, not only in EMI shielding, but also in flexible electrodes, sensors and tissue engineering scaffolds.

References

Abbasi, H., Antunes, M., & Velasco, J. I. (2019). Recent advances in carbon-based polymer nanocomposites for electromagnetic interference shielding. Progress in Materials Science, 103, 319-373.

Altaner, C. M., Thomas, L. H., Fernandes, A. N., & Jarvis, M. C. (2014). How cellulose stretches: Synergism between covalent and hydrogen bonding. Biomacromolecules, 15(3), 791-798.

Ayad, M. M. (1994). Influence of HCL on polypyrrole films prepared chemically from ferric chloride. Journal of Polymer Science Part A: Polymer Chemistry, 32(1), 9-14.

Babayan, V., Kazantseva, N. E., Moučka, R., & Stejskal, J. (2017). Electromagnetic shielding of polypyrrole-sawdust composites: Polypyrrole globules and nanotubes. Cellulose, 24(8), 3445-3451.

Ćirić-Marjanović, G., Mentus, S., Pašti, I., Gavrilov, N., Krstić, J., Travas-Sejdic, J., & Stejskal, J. (2014). Synthesis, characterization, and electrochemistry of nanotubular polypyrrole and polypyrrole-derived carbon nanotubes. The Journal of Physical Chemistry C, 118(27), 14770-14784.

Du, X., Zhang, Z., Liu, W., & Deng, Y. (2017). Nanocellulose-based conductive materials and their emerging applications in energy devices - A review. Nano Energy, 35, 299-320.

Ebrahimi, I., & Gashti, M. P. (2018). Polypyrrole-MWCNT-ag composites for electromagnetic shielding: Comparison between chemical deposition and UV-reduction approaches. Journal of Physics and Chemistry of Solids, 118, 80-87.

Gill, N., Gupta, V., Tomar, M., Sharma, A. L., Pandey, O. P., & Singh, D. P. (2020). Improved electromagnetic shielding behaviour of graphene encapsulated polypyrrole-graphene nanocomposite in X-band. Composites Science and Technology, 192, Article 108113.

Goel, S., Mazumdar, N. A., & Gupta, A. (2010). Synthesis and characterization of polypyrrole nanofibers with different dopants. Polymers for Advanced Technologies, 21(3), 205-210.

Gopakumar, D. A., Pai, A. R., Pottathara, Y. B., Pasquini, D., Carlos de Morais, L., Luke, M., & Thomas, S. (2018). Cellulose nanofiber-based polyaniline flexible papers as sustainable microwave absorbers in the X-band. ACS Applied Materials & Interfaces, 10(23), 20032-20043.

Gopakumar, D. A., Pai, A. R., Pottathara, Y. B., Pasquini, D., de Morais, L. C., Khalil, H. P. S. A., & Thomas, S. (2021). Flexible papers derived from polypyrrole deposited cellulose nanofibers for enhanced electromagnetic interference shielding in gigahertz frequencies. Journal of Applied Polymer Science, 138(16), 50262.

Granato, F., Bianco, A., Bertarelli, C., & Zerbi, G. (2009). Composite polyamide 6/ polypyrrole conductive nanofibers. Macromolecular Rapid Communications, 30(6), 453-458.

Han, H., & Cho, S. (2018). Ex situ fabrication of polypyrrole-coated Core-Shell nanoparticles for high-performance coin cell supercapacitor. Nanomaterials, 8(9), 726.

Hawkins, S. J., & Ratcliffe, N. M. (2000). A study of the effects of acid on the polymerisation of pyrrole, on the oxidative polymerisation of pyrrole and on polypyrrole. Journal of Materials Chemistry, 10(9), 2057-2062.

Hu, S., Zhou, Y., Zhang, L., Liu, S., Cui, K., Lu, Y., & Li, X. (2018). Effects of indigo carmine concentration on the morphology and microwave absorbing behavior of PPy prepared by template synthesis. Journal of Materials Science, 53(4), 3016-3026.

Huang, H.-D., Liu, C.-Y., Zhang, L.-Q., Zhong, G.-J., & Li, Z.-M. (2015). Simultaneous reinforcement and toughening of carbon Nanotube/Cellulose conductive nanocomposite films by interfacial hydrogen bonding. ACS Sustainable Chemistry & Engineering, 3(2), 317-324.

Huang, H.-D., Liu, C.-Y., Zhou, D., Jiang, X., Zhong, G.-J., Yan, D.-X., & Li, Z.-M. (2015). Cellulose composite aerogel for highly efficient electromagnetic interference shielding. Journal of Materials Chemistry A, 3(9), 4983-4991.

Huo, Y., Guo, D., Yang, J., Chang, Y., Wang, B., Mu, C., & Wen, F. (2022). Multifunctional bacterial cellulose Nanofibers/Polypyrrole (PPy) composite films for joule heating and electromagnetic interference shielding. ACS Applied Electronic Materials, 4(5), 2552-2560.

Cho, S. J., Choo, K., Kim, D. P., & Kim, J. W. (2007). H2 sorption in HCl-treated polyaniline and polypyrrole. Catalysis Today, 120(3), 336-340.

Chung, D. D. L. (2001). Electromagnetic interference shielding effectiveness of carbon materials. Carbon, 39(2), 279-285.

Chung, D. D. L. (2020). Materials for electromagnetic interference shielding. Materials Chemistry and Physics, 255.

Jiang, D., Murugadoss, V., Wang, Y., Lin, J., Ding, T., Wang, Z., & Guo, Z. (2019). Electromagnetic interference shielding polymers and nanocomposites - A review. Polymer Reviews, 59(2), 280-337.

Johnston, J., Moraes, J., & Borrmann, T. (2005). Conducting polymers on paper fibres. Synthetic Metals, 153, 65-68.

Jradi, K., Bideau, B., Chabot, B., & Daneault, C. (2012). Characterization of conductive composite films based on TEMPO-oxidized cellulose nanofibers and polypyrrole. Journal of Materials Science, 47(8), 3752-3762.

Kopecký, D., Varga, M., Prokeš, J., Vrňata, M., Trchová, M., Kopecká, J., & Václavík, M. (2017). Optimization routes for high electrical conductivity of polypyrrole nanotubes prepared in presence of methyl orange. Synthetic Metals, 230, 89-96.

Kumar, P., Narayan Maiti, U., Sikdar, A., Kumar Das, T., Kumar, A., & Sudarsan, V. (2019). Recent advances in polymer and polymer composites for electromagnetic interference shielding: Review and future prospects. Polymer Reviews, 59(4), 687-738.

Lapka, T., Kopecký, D., Mazúr, P., Prokeš, J., Ulbrich, P., Dendisová, M., & Hassouna, F. (2021). Elaboration and properties of nanofibrillated cellulose composites with polypyrrole nanotubes or their carbonized analogs. Synthetic Metals, 278, Article 116806.

Lay, M., Méndez, J. A., Delgado-Aguilar, M., Bun, K. N., & Vilaseca, F. (2016). Strong and electrically conductive nanopaper from cellulose nanofibers and polypyrrole. Carbohydrate Polymers, 152, 361-369.

Lay, M., Méndez, J. A., Pelach, M.A., Bun, K. N., & Vilaseca, F. (2016). Combined effect of carbon nanotubes and polypyrrole on the electrical properties of cellulose-nanopaper. Cellulose, 23(6), 3925-3937.

Liu, K., Du, H., Liu, W., Zhang, M., Wang, Y., Liu, H., & Si, C. (2022). Strong, flexible, and highly conductive cellulose nanofibril/PEDOT:PSS/MXene nanocomposite films for efficient electromagnetic interference shielding. Nanoscale, 14(40), 14902-14912.

Maity, S., & Chatterjee, A. (2016). Conductive polymer-based electro-conductive textile composites for electromagnetic interference shielding: A review. Journal of Industrial Textiles, 47(8), 2228-2252.

Mäkelä, T., Pienimaa, S., Taka, T., Jussila, S., & Isotalo, H. (1997). Thin polyaniline films in EMI shielding. Synthetic Metals, 85(1), 1335-1336.

Marins, J. A., Soares, B. G., Fraga, M., Muller, D., & Barra, G. M. O. (2014). Selfsupported bacterial cellulose polyaniline conducting membrane as electromagnetic interference shielding material: Effect of the oxidizing agent. Cellulose, 21 (3), 1409-1418.

Mathur, P., & Raman, S. (2020). Electromagnetic interference (EMI): Measurement and reduction techniques. Journal of Electronic Materials, 49(5), 2975-2998.

Minisy, I. M., Acharya, U., Kobera, L., Trchováa, M., Unterweger, C., Breitenbach, S., & Bober, P. (2020). Highly conducting 1-D polypyrrole prepared in the presence of safranin. Journal of Materials Chemistry C, 8(35), 12140-12147.

Minisy, I. M., Gavrilov, N., Acharya, U., Moraávkovaá, Z., Unterweger, C., Micusík, M., & Bober, P. (2019). Tailoring of carbonized polypyrrole nanotubes core by different polypyrrole shells for oxygen reduction reaction selectivity modification. Journal of Colloid and Interface Science, 551, 184-194.

Moohan, J., Stewart, S. A., Espinosa, E., Rosal, A., Rodriguez, A., Lanaieta, E., & Domínguez-Robles, J. (2020). Cellulose nanofibers and other biopolymers for biomedical applicationsA Review. Applied Sciences, 10(1), 65.

Moon, R. J., Martini, A., Nairn, J., Simonsen, J., & Youngblood, J. (2011). Cellulose nanomaterials review: Structure, properties and nanocomposites. Chemical Society Reviews, 40(7), 3941-3994.

Moučka, R., Sedlačík, M., Kasparyan, H., Prokeš, J., Trchová, M., Hassouna, F., & Kopecký, D. (2020). One-dimensional nanostructures of polypyrrole for shielding of electromagnetic interference in the microwave region. International Journal of Molecular Sciences, 21(22), 8814.

Moučka, R., Sedlačík, M., Prokes, J., Kasparyan, H., Valtera, S., & Kopecký, D. (2020). Electromagnetic interference shielding of polypyrrole nanostructures. Synthetic Metals, 269, Article 116573.

Müler, D., Rambo, C. R., Recouvreux, D. O. S., Porto, L. M., & Barra, G. M. O. (2011). Chemical in situ polymerization of polypyrrole on bacterial cellulose nanofibers. Synthetic Metals, 161(1), 106-111.

Parit, M., Du, H., Zhang, X., Prather, C., Adams, M., & Jiang, Z. (2020). Polypyrrole and cellulose nanofiber based composite films with improved physical and electrical properties for electromagnetic shielding applications. Carbohydrate Polymers, 240, Article 116304.

van der Pauw, L. J. (1958). A method of measuring specific resistivity and Hall effect of discs of arbitrary shape. Philips Research Reports, 13, 1-9.

Petit-Conil, M., Sasso, C., Beneventi, D., Chaussy, D., Zeno, E., Nortier, P., & Belgacem, N. (2011). Polypyrrole and polypyrrole/wood-derived materials conducting composites: A review. Bioresources, 6, 3585-3620.

Siqueira, G., Bras, J., & Dufresne, A. (2010). Cellulosic bionanocomposites: A review of preparation, properties and applications. Polymers, 2.

Stejskal, J., & Trchová, M. (2018). Conducting polypyrrole nanotubes: A review. Chemical Papers, 72(7), 1563-1595.

Tang, L., Han, J., Jiang, Z., Chen, S., & Wang, H. (2015). Flexible conductive polypyrrole nanocomposite membranes based on bacterial cellulose with amphiphobicity. Carbohydrate Polymers, 117, 230-235.

Thomassin, J.-M., Jérome, C., Pardoen, T., Bailly, C., Huynen, I., & Detrembleur, C. (2013). Polymer/carbon based composites as electromagnetic interference (EMI) shielding materials. Materials Science and Engineering: R: Reports, 74(7), 211-232.

Tjahyono, A. P., Aw, K. C., & Travas-Sejdic, J. (2012). A novel polypyrrole and natural rubber based flexible large strain sensor. Sensors and Actuators B: Chemical, 166-167, 426-437.

Varga, M., Kopecký, D., Kopecká, J., Křivka, I., Hanuš, J., Zhigunov, A., & Prokeš, J. (2017). The ageing of polypyrrole nanotubes synthesized with methyl orange. European Polymer Journal, 96, 176-189.

Varshney, S., Ohlan, A., Jain, V. K., Dutta, V. P., & Dhawan, S. K. (2014). Synthesis of ferrofluid based nanoarchitectured polypyrrole composites and its application for electromagnetic shielding. Materials Chemistry and Physics, 143(2), 806-813.

Wang, M., Miao, X., Li, H., & Chen, C. (2022). Effect of length of cellulose nanofibers on mechanical reinforcement of polyvinyl alcohol. Polymers, 14(1), 128.

Xie, A., Wu, F., Jiang, W., Zhang, K., Sun, M., & Wang, M. (2017). Chiral induced synthesis of helical polypyrrole (PPy) nano-structures: A lightweight and high-performance material against electromagnetic pollution. Journal of Materials Chemistry C, 5(8), 2175-2181.

Yang, W., Gong, Y., Zhao, X., Liu, T., Zhang, Y., Chen, F., & Fu, Q. (2019). Strong and highly conductive graphene composite film based on the nanocellulose-assisted dispersion of expanded graphite and incorporation of poly(ethylene oxide). ACS Sustainable Chemistry & Engineering, 7(5), 5045-5056.

Yang, W., Zhang, Y., Liu, T., Huang, R., Chai, S., Chen, F., & Fu, Q. (2017). Completely green approach for the preparation of strong and highly conductive graphene composite film by using nanocellulose as dispersing agent and mechanical compression. ACS Sustainable Chemistry & Engineering, 5(10), 9102-9113.

Yildiz, Z., Usta, I., & Gungor, A. (2012). Electrical properties and electromagnetic shielding effectiveness of polyester yarns with polypyrrole deposition. Textile Research Journal, 82(20), 2137-2148.